Science Advances
AAAS

advances.sciencemag.org/cgi/content/full/4/11/eaau2104/DC1

# Supplementary Materials for

## Dynamic assembly of liquid crystalline graphene oxide gel fibers for ion transport

H. Park, K. H. Lee, Y. B. Kim, S. B. Ambade, S. H. Noh, W. Eom, J. Y. Hwang, W. J. Lee*, J. Huang*, T. H. Han*

*Corresponding author. Email: than@hanyang.ac.kr (T.H.H.); jiaxing-huang@northwestern.edu (J.H.); wjlee@dankook.ac.kr (W.J.L.)

Published 2 November 2018, *Sci. Adv.* **4**, eaau2104 (2018)
DOI: 10.1126/sciadv.aau2104

**The PDF file includes:**



**Other Supplementary Material for this manuscript includes the following:**

(available at advances.sciencemag.org/cgi/content/full/4/11/eaau2104/DC1)

Movie S1 (.mp4 format). In situ observation of dynamic assembly of GO gel fiber at $v_2 = v_1$.
Movie S2 (.mp4 format). In situ observation of dynamic assembly of GO gel fiber at $v_2 = 3v_1$.

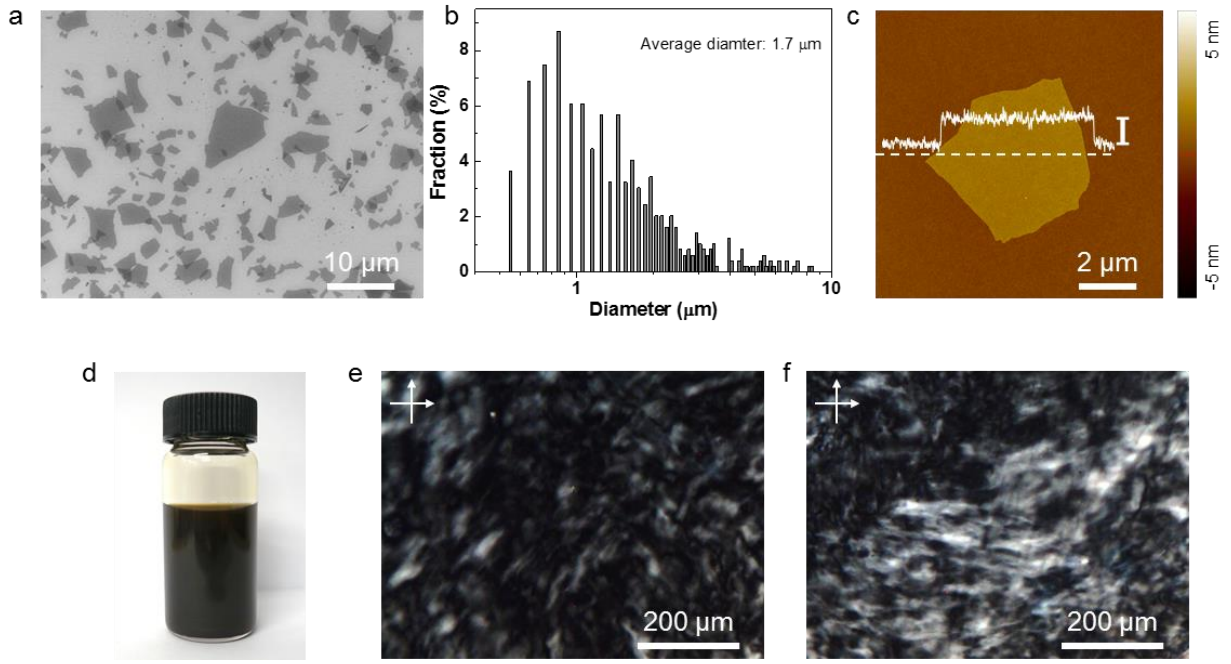


**Fig. S1. Characterization of GOLC dispersion.** (**a**) A typical SEM image of GO sheets. (**b**) Size distribution of the GO sheets. (**c**) A typical atomic force microscopy (AFM) image of GO sheet. The scale bar (I) denotes 1.6 nm of height. From the uniform thickness and average lateral size (1.7 μm), the aspect ratio of GO sheet was calculated to be $1.07 \times 10^3$ and is in the range of previously reported values (700-2600) of GO with high liquid crystallinity (*14*, *39*). (**d**) A digital photo of typical GOLC dispersion (0.5 wt%) used for the gel-fiber assembly. (**e**-**f**) POM images of GOLC dispersion with 0.5 and 1.0 wt%, respectively.

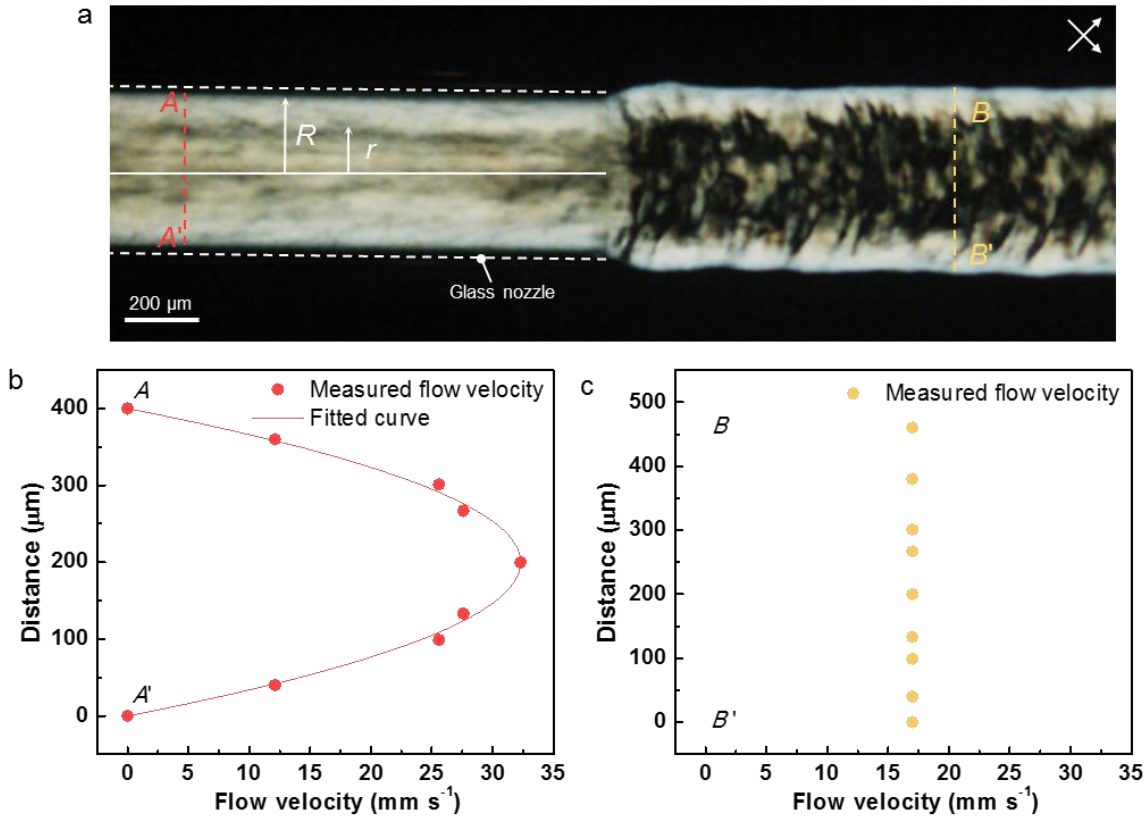


**Fig. S2. Analysis of velocity profile.** (**a**) Expanded POM image of 1st one in **Fig. 1c** showing two dotted lines; *A*-*A*' (inside the nozzle) and *B*-*B*' (in the ejected fluid). (**b**) Experimental and fitted flow velocity of GOLC fluid inside the nozzle as a function of distance showing a parabolic velocity profile. (**c**) Experimental velocity profile of ejected fluid at $v_2 = v_1$.

**Note**: The parabolic velocity profile in (b) was fitted with the following equation: $v_0(r) = v_{0,\,max}(1 - r^2/R^2)$, where $v_0(r)$ is the velocity of the GOLC fluid depending on radial location ($r$) in the nozzle. $R$ and $v_{0,\,max}$ are the radius of the nozzle (200 μm) and the maximum velocity (32 mm $s^{-1}$) of the fluid at $r = 0$.

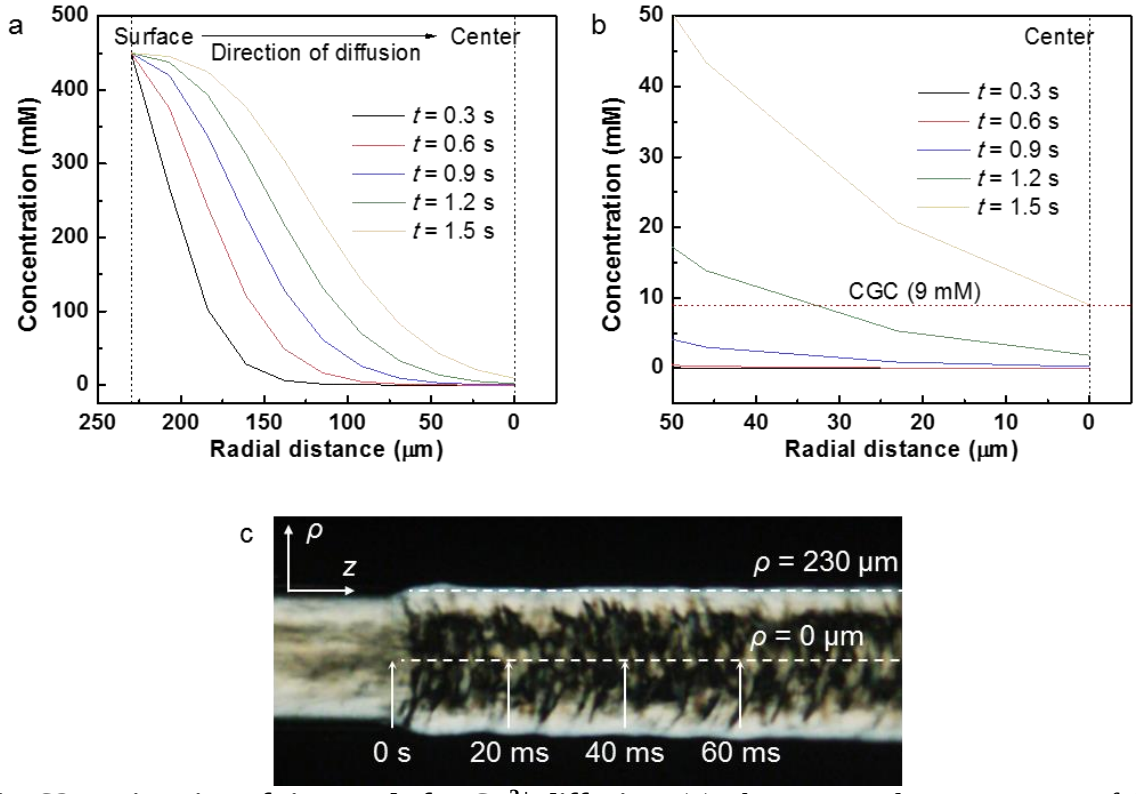


**Fig. S3. Estimation of time scale for $Ca^{2+}$ diffusion.** (**a**) The estimated concentration of $Ca^{2+}$ ($C$) as a function of radial distance ($\rho$) for the diffusion into the ejected fluid at $v_2 = v_1$. (**b**) The estimated concentration at the core region (0 μm $\leq \rho \leq$ 50 μm). The critical gelation concentration (CGC) of $Ca^{2+}$ (9 mM) is highlighted with a red dotted line. (**c**) 1st POM image in **Fig. 1c** showing the elapsed time after ejection at each axial position ($z$).

**Note**: The diffusion time scale of $Ca^{2+}$ ($t$) was estimated as solving the diffusion equation in cylindrical coordinates

$$\frac{\partial C}{\partial t} = \frac{1}{\rho}\frac{\partial}{\partial \rho}\left(\rho D \frac{\partial C}{\partial \rho}\right) \tag{1}$$

where $D$, $C$, and $\rho$ are the diffusion coefficient of $Ca^{2+}$ ($0.79 \times 10^{-5}$ $cm^2$ $s^{-1}$), the concentration of $Ca^{2+}$, and radial distance from the center of ejected fluid, respectively. In our system, the cations ($Ca^{2+}$) diffuse from near the surface ($\rho_{surface}$ = 230 μm; $C_{surface}$ = 450 mM) to the center ($\rho_{center}$ = 0 μm; $C_{center}$ = 0 M) by the large concentration gradient (1st image in **Fig. 1c**). Thus, the boundary conditions are as follows

$$C(\rho_{surface}, t) = C_{surface} \tag{2}$$

$$\frac{\partial C}{\partial \rho}\left(\rho_{center}, t\right) = 0 \tag{3}$$

We plotted the estimated $C$ as a function of $\rho$ (**Fig. S3a** and **b**). The critical concentration of $Ca^{2+}$ for the gelation of GO was chosen to 9 mM based on a previous report (*40*). As shown in **fig. S3b**, the time required for fully gelling the ejected fluid was estimated to be ~1.5 s.

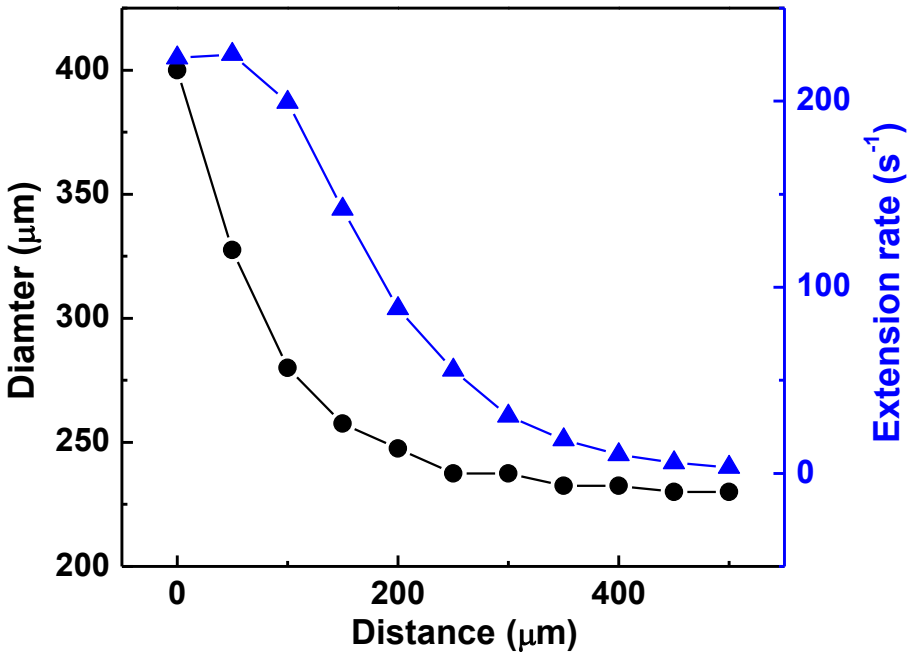


**Fig. S4. Diameter and extension rate of ejected fluid at $v_2 = 5.5v_1$ as a function of distance.**

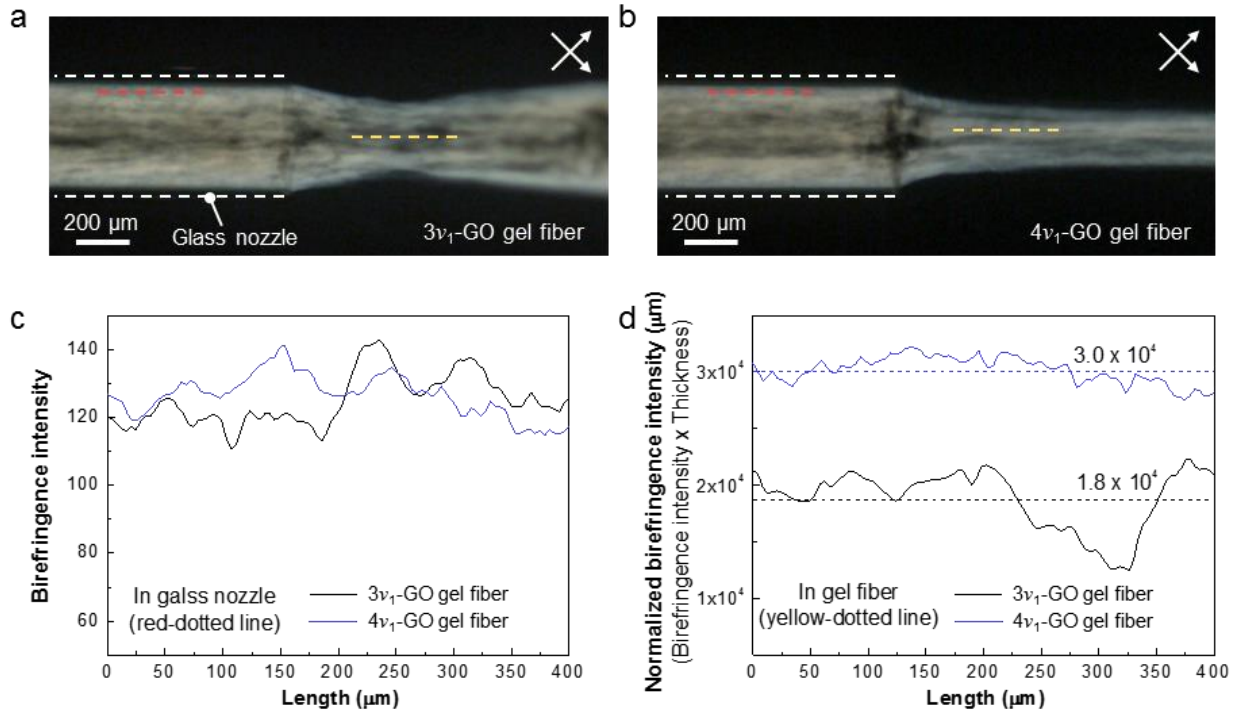


**Fig. S5. POM images and birefringence intensity profiles of gel fibers.** (**a-b**) POM images of a (a) 3$v_1$-GO gel fiber and (b) 4$v_1$-GO gel fiber, respectively. (**c**) Birefringence intensity profile along the red lines in the glass nozzle for (a) and (b). (**d**) Normalized birefringence intensity profile along the yellow lines for (a) and (b). The dashed lines in (d) denote mean values.

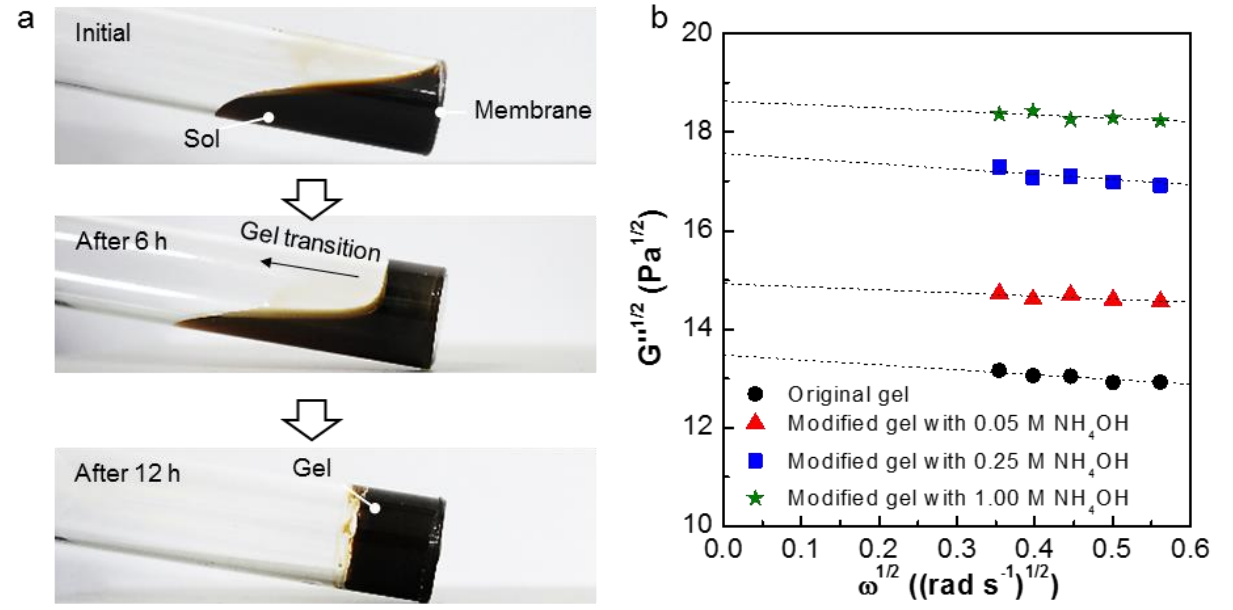


**Fig. S6. Sol-gel transition and gel behavior of GO solution.** (**a**) Series of photographs showing the sol-gel transition of GO dispersion started from the membrane interface and propagated normal to the membrane plane. Finally, GO dispersion was fully converted to a gel after 12 h. (**b**) Casson plots of GO gels prepared with different amount of the added $NH_4OH$ in 5 wt% $CaCl_2$ coagulation solution.

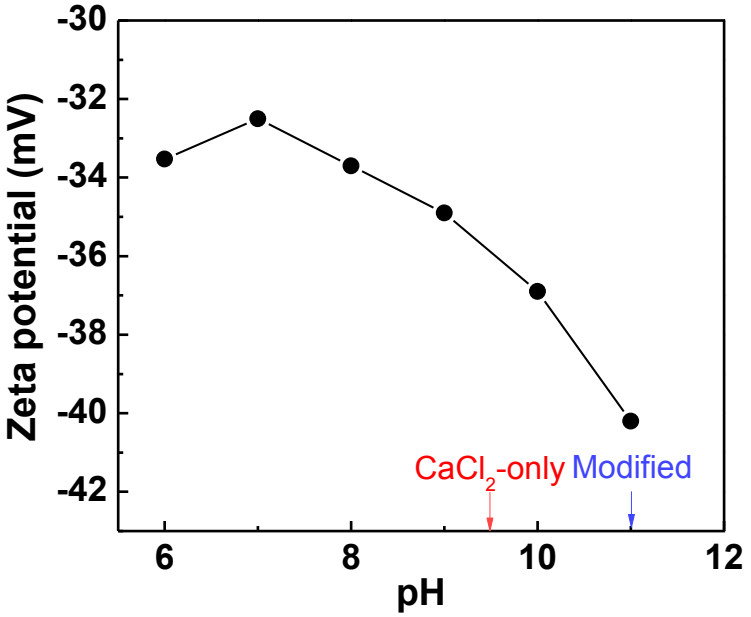


**Fig. S7. Zeta potential of GO as a function of pH in aqueous dispersion at a concentration of 0.05 mg ml$^{-1}$.** The red and blue arrows denote the pH values of $CaCl_2$-only (9.5) and modified (11) coagulation solution.

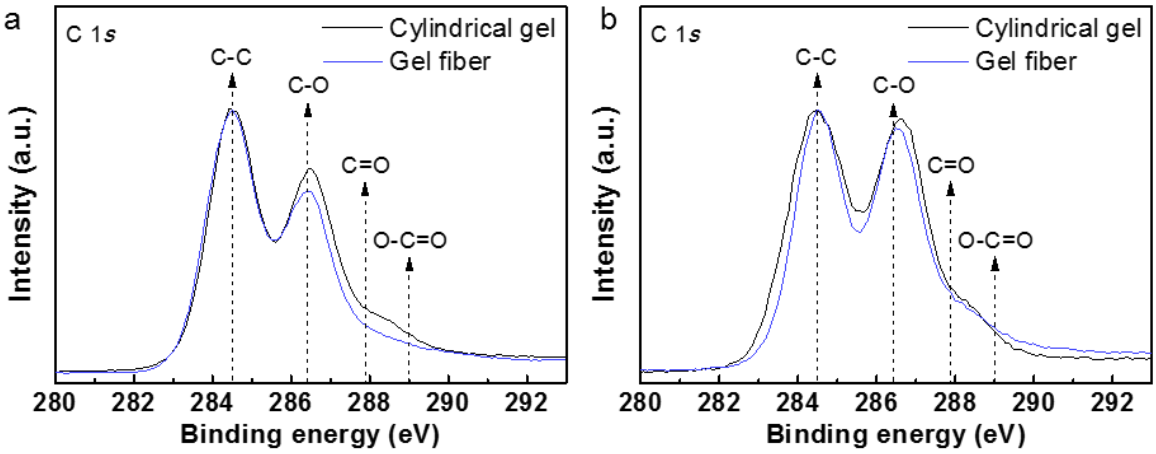


**Fig. S8. XPS spectra of GO gels.** High resolution C 1*s* spectra in XPS of cylindrical gels and gel fibers coagulated in (**a**) modified and (**b**) $CaCl_2$-only coagulation solution, respectively.

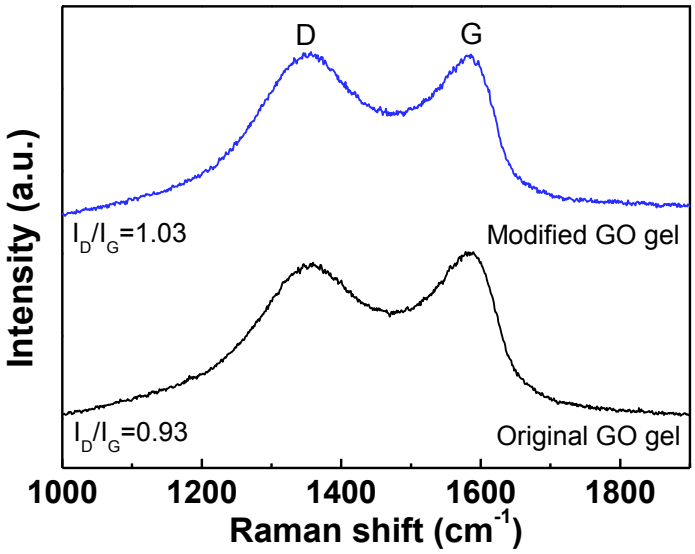


**Fig. S9. Raman spectra of GO gels.**

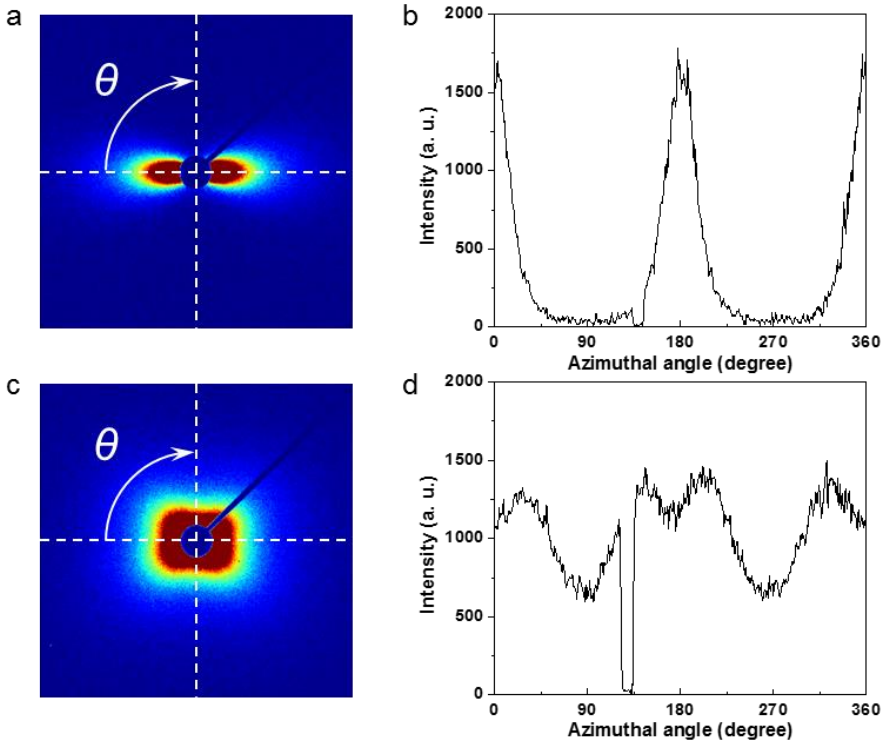


**Fig. S10. Determination of the degree of orientation in gel fibers.** (**a**-**c**) SAXS patterns of 4$v_1$- and $v_1$-GO gel fibers, respectively. (**b**-**d**) Corresponding azimuthal scans used to determine the degree of orientation in the gel fibers.

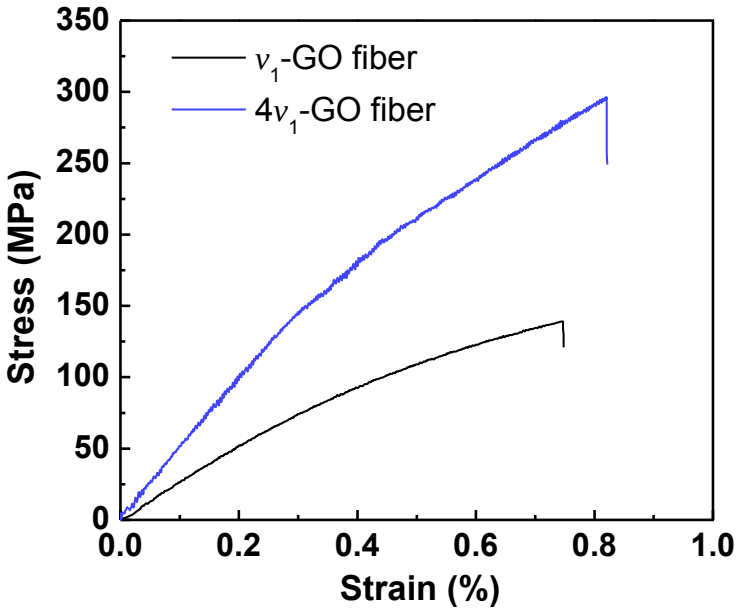


**Fig. S11. Stress-strain curves of dried GO fibers under 10% min$^{-1}$ of tensile strain.**

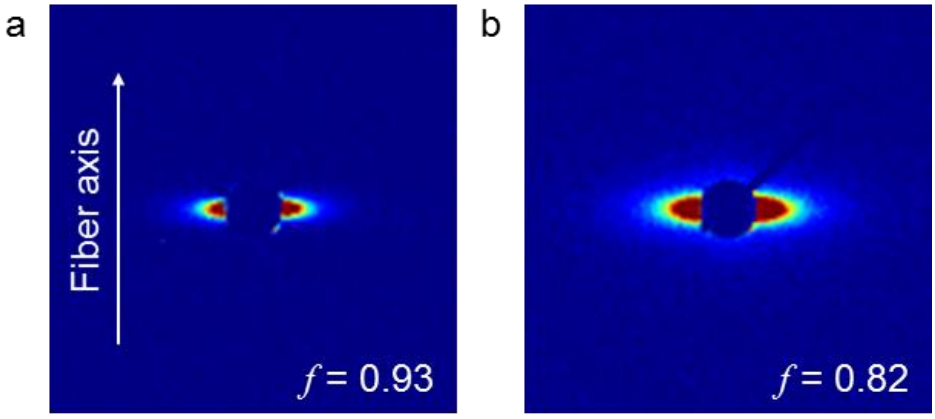


**Fig. S12. Determination of the degree of orientation in dried fibers.** (**a-b**) 2D SAXS patterns of (a) $4v_1$- and (b) $v_1$-GO fibers, respectively. $f$ denotes Herman's orientation function.

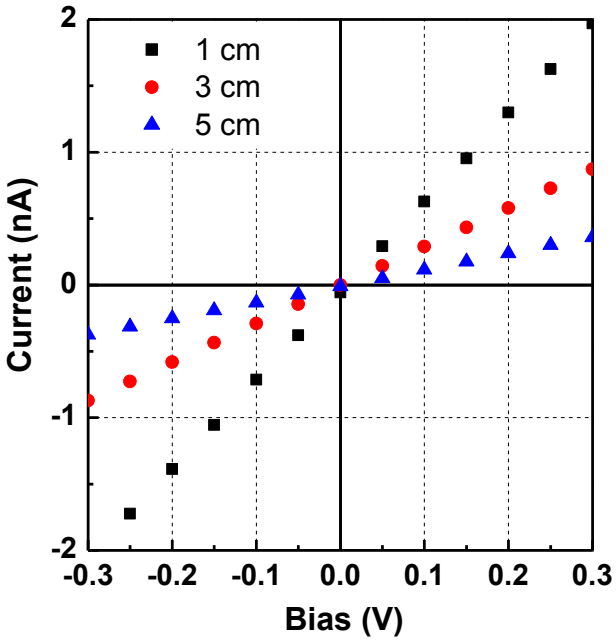


**Fig. S13. *I*-*V* curves of NICs of different lengths.**

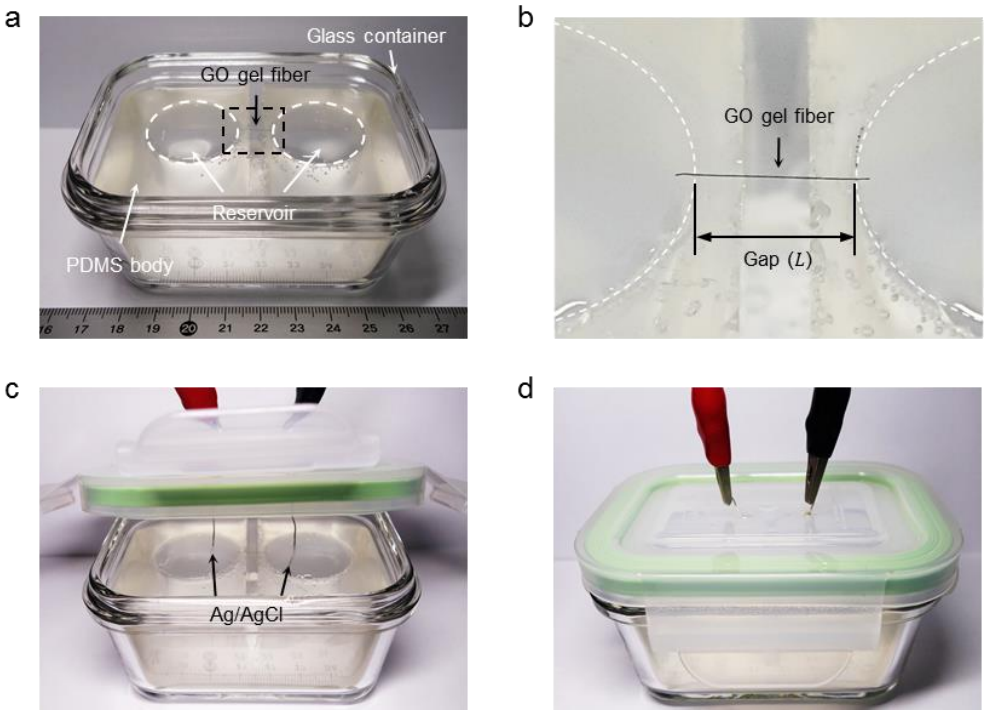


**Fig. S14. Experimental setup for measuring the ionic conductivity of NICs.** (**a**) A digital photo of a typical PDMS cell, consisting of both source and drain reservoirs with a 10 mm-length gap between them. (**b**) A magnified photo of the black box in (a) showing a GO gel fiber bridging the two reservoirs. (**c**-**d**) The measurement cell was sealed in a glass container and connected to a potentiostat using Ag/AgCl electrodes. Photo credit: Ki Hyun Lee, Hanyang University, Dept. of Organic and Nano Engineering.

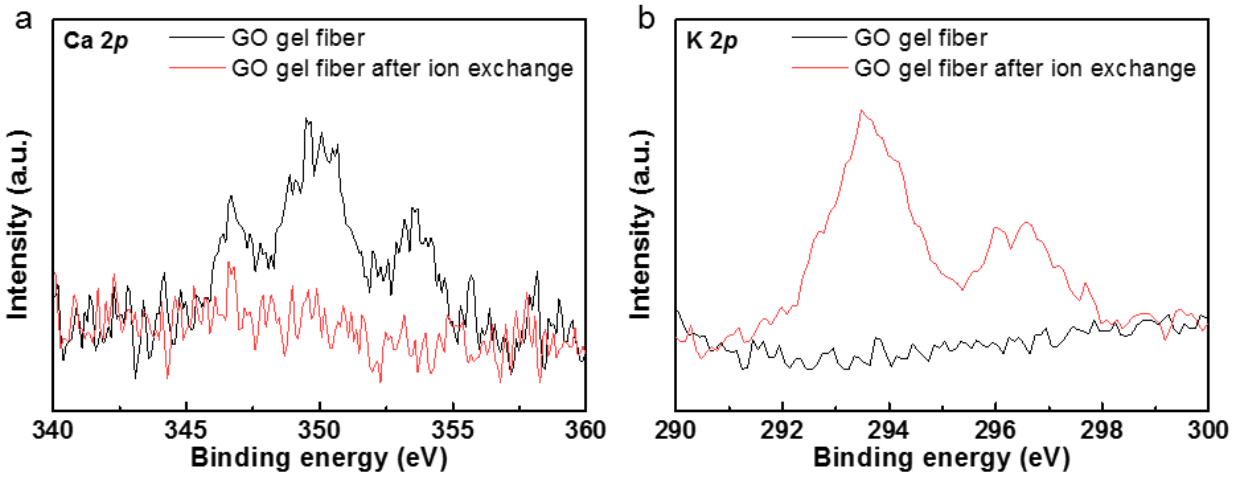


**Fig. S15. Removal of $Ca^{2+}$ by ion exchange in GO gel fibers.** (**a**-**b**) High resolution Ca 2*p* and K 2*p* curves of GO gel fibers in XPS before and after KCl treatment, respectively, suggesting removal of $Ca^{2+}$ and exchange for $K^{+}$.

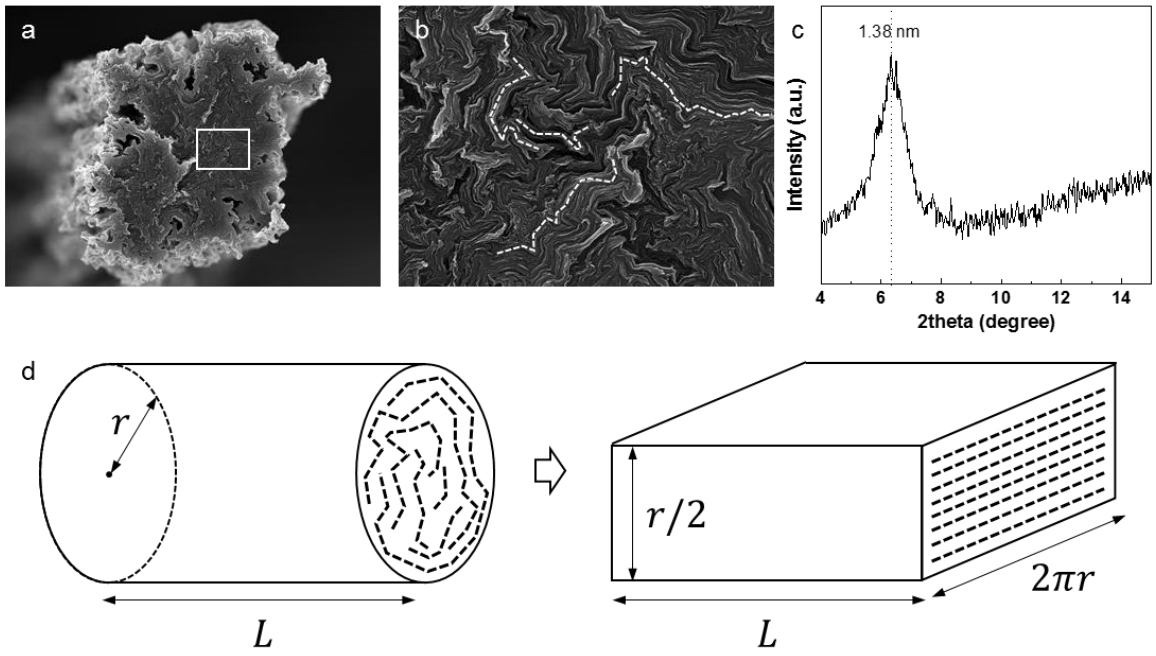


**Fig. S16. Modeling of GO gel fiber nanochannels using the configuration of GO films.** (**a**) A typical SEM image of the cross-sectional view of a dried GO gel fiber. (**b**) Magnified image of the white box in (a). Dotted lines represent some curved 2D nanochannels in the GO gel fiber. (**c**) XRD patterns of GO gel fibers, indicating an interlayer spacing of 1.38 nm after rehydration in KCl solution. (**d**) Schematic illustration of re-assembly of nanochannels confined in a cylindrical fiber with radius (*r*); this was converted into a rectangular parallelepiped as is performed for GO films.

**Table S1. Yield stress values of GO gels prepared with different amounts of $NH_4OH$.**

| | Original GO gel | Modified GO gel | | |
|---|---|---|---|---|
| | | 0.05 M $NH_4OH$ | 0.25 M $NH_4OH$ | 1.00 M $NH_4OH$ |
| Yield stress [Pa] | 181 | 222 | 308 | 346 |

**Table S2. Quantitative XPS analyses of cylindrical gels and gel fibers.**

| Sample | Coagulation solution | C [at%] | O [at%] | Ca [at%] | O/C ratio | Ca/C ratio |
|---|---|---|---|---|---|---|
| Cylindrical gel | $CaCl_2$ only | 65.9 | 33.0 | 1.1 | 0.50 | 0.016 |
| | $CaCl_2$, $NH_4OH$ | 68.1 | 29.6 | 2.3 | 0.43 | 0.034 |
| Gel fiber | $CaCl_2$ only | 65.2 | 33.9 | 0.9 | 0.52 | 0.014 |
| | $CaCl_2$, $NH_4OH$ | 69.6 | 27.6 | 2.8 | 0.40 | 0.040 |

**Table S3. Comparison of mechanical properties of our GO fibers with previously reported GO fibers and other nanocarbon-based fibers.**

| Sample | Young's modulus [GPa] | Tensile strength [MPa] | Elongation at break [%] | Draw ratio | Degree of orientation | Method | Note |
|---|---|---|---|---|---|---|---|
| $v_1$-GO fiber | 27.6 ± 7.3 | 152.3 ± 36.0 | 0.7 ± 0.2 | 1 | 0.82 | Wet spinning | this work |
| $4v_1$-GO fiber | 38.3 ± 1.7 | 301.4 ± 52.9 | 0.8 ± 0.1 | 4 | 0.93 | Wet spinning | |
| GO fiber with large GO (18.5 μm of mean size) | 6.3 | 364.4 | 6.8 | 1.3 | - | Wet spinning | Ref. *42* |
| GO fiber with large GO (56 ± 20 μm of mean size) | 12.1 | 239.3 | 2.7 | 1.2 | - | Wet spinning | Ref. *43* |
| Knittable GO fiber | 7.9 | 135.8 | 5.9 | - | - | Dry-jet wet spinning | Ref. *44* |
| Double-walled carbon nanotube (DWCNT) fiber | 8.3 | 299 | 5 | - | - | Drawing-drying process | Ref. *45* |
| Nanocelluose fiber | 21.3 ± 5.5 | 296 ± 71 | 2.8 ± 0.5 | 1 | 0.83 | Wet spinning | Ref. *46* |
| Nanocelluose fiber* | 17.6 ± 0.7 | 490 ± 86 | 6.4 ± 1.6 | 1.15 | 0.50 ± 0.01 | Hydrodynamic assembly | Ref. *18* |
| Nanocelluose fiber | 86 | 1570 | ~3 | - | 0.70 | Hydrodynamic assembly | Ref. 47 |
| Graphene nanoribbon fiber (annealed at 1300 °C) | 15.3 ± 1.0 | 151.7 ± 20.7 | 1.02 ± 0.21 | - | 0.53 | Dry-jet wet spinning | Ref. *48* |

*It should be noted that the diffusion time scale in Ref. *16* is 3.3 s.

**Table S4. Structural parameters of dried GO fibers.**

| Sample | Diameter [μm] | Linear density [Tex] | Apparent volume fraction [%] | Apparent porosity [%] | Apparent density [g $cm^{-3}$] |
|---|---|---|---|---|---|
| $v_1$-GO fiber | 26.8 ± 1.4 | 0.70 ± 0.07 | 69 | 31 | 1.24 |
| $4v_1$-GO fiber | 14.3 ± 0.5 | 0.23 ± 0.01 | 80 | 20 | 1.43 |

**Note**: The apparent volume fraction, porosity, and density were calculated using previously reported density (1.8 g $cm^{-3}$) of GO (*41*) by assuming the geometry of fiber is a cylinder.

**Table S5. Comparison of ionic conductivity of GO gel fibers with various nanosheet films.**

| Sample | Building block | Electrolyte | Ionic conductivity [S $cm^{-1}$] | Note |
|---|---|---|---|---|
| $v_1$-GO gel fiber | GO | < 3 mM KCl | $1.7 \times 10^{-4}$ | this work |
| $4v_1$-GO gel fiber | GO | < 7 mM KCl | $4.2 \times 10^{-4}$ | |
| GO film | GO | < 10 mM KCl | ~$1.0 \times 10^{-3}$ | Ref. *7* |
| Boron nitride (BN) film | BN sheets | < 0.1 mM KCl | ~$1.0 \times 10^{-4}$ | Ref. *49* |
| Vermiculite film | Vermiculite sheet | < 0.1 M HCl | $6.0 \times 10^{-3}$ | Ref. *50* |